Three-Degree-of-Freedom Wind Tunnel Results Employing Rate Gyros

G.T. Chrusciel*
Lockheed Missiles & Space Company, Inc., Sunnyvale, Calif.

Results of a three-degree-of-freedom dynamic test performed at Mach 10 for an asymmetric nose modification of a slender, spherically blunted cone are presented. Angle-of-attack data obtained directly from the dynamic balance are compared with results independently determined from onboard rate gyro information telemetered from the model. Gyro-derived aerodynamic moments acting in the wind vector plane and out-of-plane orientations are compared with results obtained from static and one-degree-of-freedom dynamic tests. The magnitude of the moment asymmetry resulting from the distorted nose and its orientation is derived every half cycle based on the out-of-plane behavior, providing the static asymmetric moment coefficient and orientation regardless of the roll frequency in relation to resonance. Results presented for three roll rates (corresponding to the ratio of roll/aerodynamic frequency $\Delta\omega/\omega_o \approx 0.3,\ 0.6,\ 1.8$) demonstrate the adequacy of the gyros and analysis technique for determining angle of attack and detailed moment behavior.

Nomenclature

C_A = axial force coefficient
C_{ℓ_0} = zero-angle-of-attack rolling moment coefficient
C_{ℓ_p} = roll damping coefficient
C_{ℓ_β} = distorted body rolling moment coefficient
C_m = total in-plane pitching moment coefficient
C_{mor} = zero-angle-of-attack pitching moment coefficient, contributions of asymmetry, $C_{\text{mor}} = [(C_{m_{oz'}})^2 + (C_{m_{0y'}})^2]^{1/2}$
$(C_{m_q} + C_{m_{\dot\alpha}})$ = damping coefficient
C_N = normal force coefficient
C_n = total out-of-plane moment coefficient
D = reference diameter, base diameter
I = moment of inertia in pitch and yaw
I_x = roll moment of inertia
M = aerodynamic moment
p,q,r = roll rate, pitch rate, yaw rate, body-fixed axis
$\bar{q}$ = freestream dynamic pressure
S = reference area, base area
t = time, from time reference
V = freestream velocity
X,Y,Z = space-fixed axes
X',Y',Z' = principal axes of inertia
x',y',z' = body-fixed axes
α,β,ϕ_A = Euler angles in wind-fixed coordinate system (referenced to velocity vector)
ϵ = magnitude of radial CG offset
η = orientation angle of resultant aerodynamic asymmetry moment axis to the z' axis, $(C_{m_{0y'}}/C_{m_{oy'}}) = \tan(\eta)$
Γ = orientation angle of radial CG offset to the z' axis—measured clockwise looking at aft end of body
v_1 = Z' moment contribution of $\epsilon, C_A \epsilon \sin(\Gamma+\phi)/D$
v_2 = Y' moment contribution of $\epsilon, C_A \epsilon \cos(\Gamma+\phi)/D$
θ,ψ,ϕ = Euler angles defined in Fig. 1
ω_0 = basic oscillation frequency
$\Delta\omega_0$ = roll frequency contribution to pitch frequency, $= p(1 - I_x/2I)$
θ',ψ',ϕ_B = three-degree-of-freedom dynamic balance referenced angles
$(\dot{})$ = time derivatives

Subscripts

x',y',z' = terms evaluated about the body-fixed axes
X',Y',Z' = terms evaluated about the principal axes of inertia
sym = symmetric body contribution

Presented as Paper 76-94 at the AIAA 14th Aerospace Sciences Meeting, Washington, D.C., Jan. 26-28, 1976; submitted Dec. 9, 1976; revision received Oct. 11, 1977.

Index categories: Entry Vehicle Dynamics and Control; Entry Vehicle Testing, Flight and Ground.

*Staff Engineer, Aerothermodynamics and Vulnerability Department. Member AIAA.

Introduction

TO date indirect approaches have been relied upon to extract aerodynamic characteristics from multi-degree-of-freedom dynamic tests (including ballistic range free-flight results). These indirect methods include: applications of the linearized epicyclic theory,[1-3] differential correction method[4] allowing for assumed forms of nonlinear aerodynamic characteristics, and improved epicyclic theory techniques.[5-7] The objectives of the present tests were to use onboard rate gyro data to: 1) directly obtain aerodynamic moment characteristics for symmetric and asymmetric configurations that can be compared with measured static and one degree-of-freedom dynamic data; 2) compare the angle of attack derived from integration of the gyro rates with that obtained directly from the three-degree-of-freedom dynamic balance; 3) demonstrate the adequacy of typical re-entry body flight test gyros for providing sufficient accuracy for analysis; and 4) evaluate a gyro analysis technique for extracting in- and out-of-plane aerodynamic moment data for symmetric and typical asymmetric re-entry configurations.

Approach

The three-degree-of-rotational-freedom plane-fixed equations of motion form the basis for analysis. This coordinate system separates out and resolves the dominant aerodynamic moments in the angle-of-attack (in-plane) from the generally smaller moments acting in the plane normal to angle-of-attack plane (out-of-plane). The following assumptions have been made in addition to the motion constraint imposed by the test apparatus: the axes for the plane-fixed coordinate system (X',Y',Z') are the principal axes of inertia for roll $(I_{X'})$, yaw $(I_{Y'})$, and pitch $(I_{Z'})$, respectively; pitch and yaw inertias are equal; and the

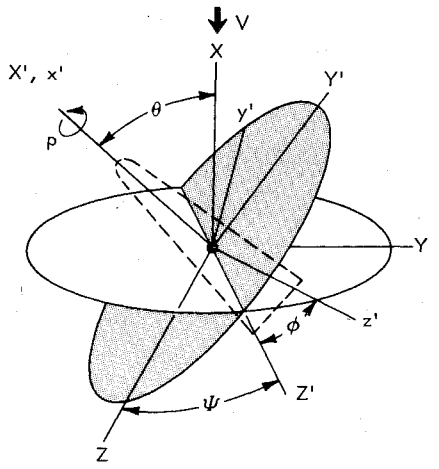

Fig. 1 Plane-fixed coordinate system.

aerodynamic centerline is aligned with the longitudinal inertia axis.

The angles ψ,θ,ϕ defining the angular motion of the wind tunnel model in the plane-fixed coordinate system are shown in Fig. 1. The X axis is aligned with the wind tunnel velocity vector. The following aerodynamic moment equations are developed from the basic relationship for the change in angular momentum in a space-fixed axis system to that of a body-fixed system:[8]

$$M_{Z'} = I\ddot{\theta} + I_x p\dot{\psi}\sin\theta - I\dot{\psi}^2\sin\theta\cos\theta = C_m \bar{q} SD \tag{1}$$

$$M_{Y'}\sin\theta = I\mathrm{d}/\mathrm{d}t(\dot{\psi}\sin^2\theta) - I_x p\sin\theta\dot{\theta} = C_n \bar{q} SD\sin\theta \tag{2}$$

$$M_{X'} = I_x\dot{p} = C_\ell \bar{q}\, SD \tag{3}$$

Time histories of $\theta,\dot{\theta},\dot{\psi}$, and p are required for the solution of Eqs. (1-3); these are provided by the body-fixed rate gyro data. However, use of the experimental data with inherent inaccuracies requires a corrective procedure in the analysis. Angles α,β,ϕ_A in a wind-fixed coordinate system are determined from the gyro information. Use of this coordinate system allows application of the assumed condition that the angular motion is centered about the velocity vector for significant aerodynamic moments relative to the inertial terms; consequently, small corrections can be applied to the data to null out errors caused by integration of the test rate data. The relationship between the two coordinate systems and expressions used to obtain the plane fixed angles and rates are described in Ref. 8. Total instantaneous moment coefficients in the angle of attack (C_m) and out-of-plane (C_n) directions are obtained from Eqs. (1) and (2) using central differences for the $\ddot{\theta}$ and $\mathrm{d}/\mathrm{d}t(\dot{\psi}\sin^2\theta)$ derivatives.

Total aerodynamic moments obtained from Eqs. (1-3) are applicable to general asymmetric as well as symmetric configurations. For asymmetric configurations that exhibit $(\mathrm{d}C_m/\mathrm{d}\theta)_\phi$ variations dependent on roll position of the body axis relative to the wind vector plane (ϕ), a large matrix of data is required to characterize the C_m and C_n moment behavior as a function of angle of attack (θ) and roll position. Examples of such geometries are: noncircular cross sections, and basic bodies of revolution employing nose geometries that produce significant distortions in the radial symmetry of the bow shock such as those created by bent noses and highly asymmetric shapes.

However, a large class of configurations can realistically be considered basic symmetric bodies with small aerodynamic asymmetries. This classification permits simplistic modeling of the asymmetry terms, thus aiding considerably in interpretation of test results for a limited range of θ and ϕ. The assumptions made for analyzing the moments derived from Eqs. (1-3) are: 1) nonlinear aerodynamic characteristics for a basic symmetric body are functions of angle of attack only; 2) a moment coefficient increment due to body asymmetry is fixed with respect to the body axis system and is independent of angle of attack and roll orientation; and 3) a radial center of gravity offset is fixed in the body axis system.

Moment results obtained from application of these assumptions are

$$C_m = C_{m_{\mathrm{sym}}} + C_{\mathrm{mor}}\cos(\eta+\phi) + \upsilon_1 + (C_{m_q} + C_{m_{\dot{\alpha}}})\dot{\theta}D/V \tag{4}$$

$$C_n = C_{\mathrm{mor}}\sin(\eta+\phi) - \upsilon_2 - (C_{m_q} + C_{m_{\dot{\alpha}}})\dot{\psi}\sin\theta D/V \tag{5}$$

$$C_\ell = C_{\ell_o} + C_{\ell_p}(pD/V) + \epsilon\cos(\Gamma+\phi)C_N/D + C_{\ell_\beta}\theta\sin(\eta+\phi) \tag{6}$$

An integrated value (over half a cycle of oscillation) of a body-fixed moment asymmetry (C_{mor}) and its orientation (η) can be obtained[8] from Eq. (5) by assuming that C_{mor} and η are constant for the time interval and by neglecting the damping and CG offset contributions.† Using the same assumptions, a derivative form of Eq. (5) provides an instantaneous result for C_{mor}, η (useful in interpreting transient moment asymmetries)

$$C_{\mathrm{mor}} = \frac{\mathrm{d}C_n/\mathrm{d}\phi - (\mathrm{d}C_{\mathrm{mor}}/\mathrm{d}\phi)\sin(\eta+\phi)}{(1+\mathrm{d}\eta/\mathrm{d}\phi)\cos(\eta+\phi)} \tag{7}$$

For C_{mor},η constants over a small time interval, Eq. (7) can be evaluated

$$C_{\mathrm{mor}} = (\mathrm{d}C_n/\mathrm{d}\phi)_{C_n=0}$$

$$\eta = 2\pi - (\phi)_{C_n=0} \text{ for } (\mathrm{d}C_n/\mathrm{d}\phi)_{C_n=0} > 0 \tag{8}$$

$$\eta = \pi - (\phi)_{C_n=0} \text{ for } (\mathrm{d}C_n/\mathrm{d}\phi)_{C_n=0} < 0$$

$C_{m_{\mathrm{sym}}}$ is obtained from Eq. (4) by using the results of Eq. (8) and assuming the damping contribution is neglible.

Test Apparatus and Data

A schematic of the test hardware employing a three-degree-of-freedom dynamic balance[9] is shown in Fig. 2. A stainless steel, 9.5-in. base diameter, 7-deg cone model was fitted with a spherically blunted tip which provided a nose-to-base radius ratio of 0.20, and an asymmetric tip simulating an ablated profile at a trim angle of attack. A sketch of the nose geometry is presented in Fig. 3. The models were statically and dynamically balanced about a CG corresponding to the center of the spherical gas bearing using balance planes located in the nose and aft end. The principal axis misalignment with respect to the aerodynamic (geometric) axis was estimated as less than 0.05 deg; the radial CG offset was controlled to within 0.002 in. The three-degree-of-freedom apparatus includes high-pressure air jets located near the aft end of the model for providing initial motion conditons and roll rate; in addition, restraining arms are provided to limit model motion.

The onboard instrumentation package consisted of a flight-quality three-axis rate gyro (pitch/yaw rates = ±100 deg/s, roll rate = −500 to +1500 deg/s), and an FM/FM telemetry system powered by a wet cell battery pack. Roll position of the model was obtained from a null in the signal strength/roll pattern of the transmitting antenna. Rate gyro and dynamic balance angular position (θ',ψ',ϕ_B) signals were carried along the sting and routed to the data acquisition system.

Small time varying biases resulted from frequency drifts in the telemetry system as a consequence of battery fluid vapor

†Order of magnitude considerations justify these assumptions for typical slender re-entry vehicle applications. Note that the CG offset contribution to C_{mor}, η can be directly obtained from C_A measurements.

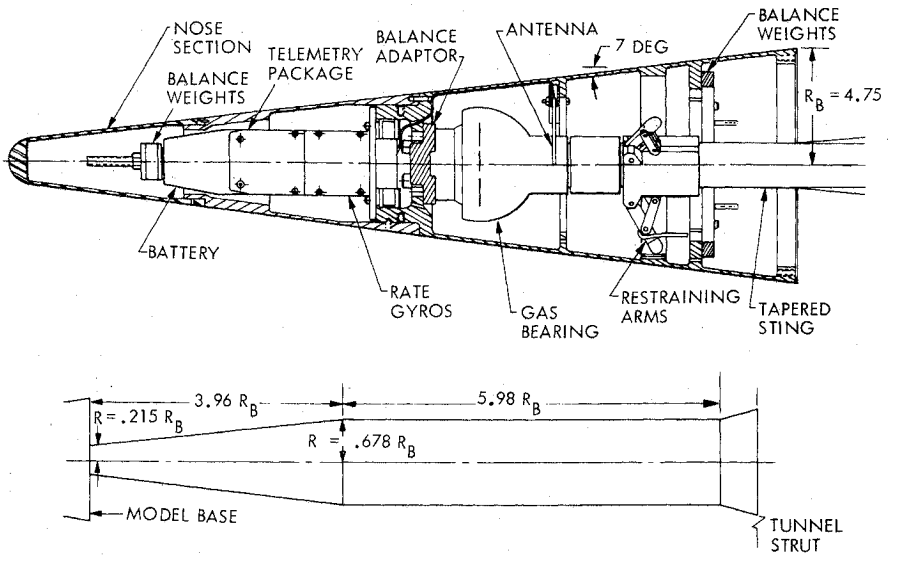

Fig. 2 Three-degree-of-freedom model and sting geometry, $R_B = 4.75$ in.

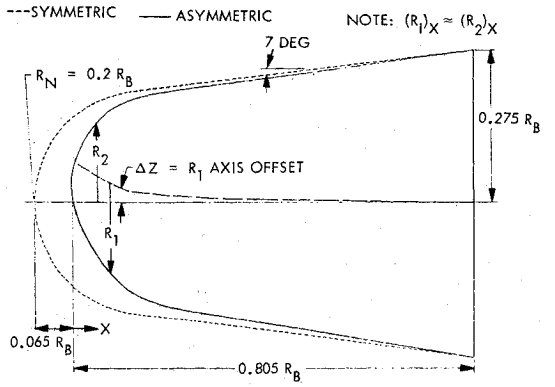

Fig. 3 Nose configurations, $R_B = 4.75$ in.

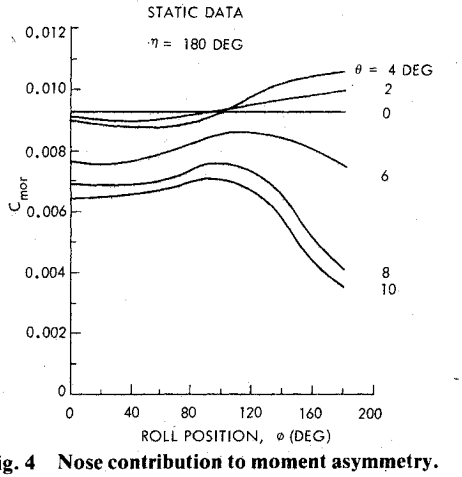

Fig. 4 Nose contribution to moment asymmetry.

leakage during the tests. Linear bias variations were obtained for pitch and yaw rates with the model motion restrained at the start and end of the runs below resonance. Since zero roll rate had not been achieved at the end of the test runs, roll rate biases were determined by an iterative procedure of matching the gyro-derived α/β angular pattern history with the dynamic balance $\theta'/-\psi'$ results. Rates for the run above resonance were not nulled at the end of the recorded data. The initial yaw bias was assumed constant, and the end pitch rate bias was determined by imposing a symmetric rate pattern. The digitized rate gyro results were smoothed using a weighting filter method to remove noise in the recorded signal. The θ'/ψ' dynamic balance angular output was processed using an inverse filter technique[10] to correct for nonlinear phase shift and amplitude attenuation caused by the low-pass filter characteristics of the facility carrier amplifiers.

The test conditions employed at Von Kármán Gas Dynamics Facility, Tunnel C, were $M = 10$, $P_o = 1800$ psia, $T_o = 1800°$R, $R_{e_D} = 1.75 \times 10^6$, and $V = 4780$ fps.

The test runs selected provide a wide range of motion patterns and roll to aerodynamic frequency ratios. The data are presented over a relatively short time period (approximately 10 cycles) to demonstrate the comparison of the dynamic balance angle-of-attack data to the gyro-derived results. Gyro analysis of detailed static and dynamic moment coefficients are compared with one-degree-of-freedom dynamic and static stability test results. All test data presented were obtained with the tapered sting depicted in Fig. 2.

Static Moment Asymmetry

For reference to the gyro-derived data, the static moment asymmetry coefficient (C_{mor}) resulting from the asymmetric nose is presented in Fig. 4 as a function of roll angle (ϕ) and total angle of attack (θ). The experimental values were obtained by applying Eqs. (4) and (5) to the in- and out-of-plane moments measured by a static balance for the symmetric and asymmetric configurations rolled through 30-deg increments. Although the asymmetric nose produces a relatively large static trim angle of approximately 1.5 deg, the moment asymmetry is essentially independent of roll angle and angle of attack for $\theta < 5$ deg validating the assumption imposed upon the analysis for a reasonable range of angle of attack relative to trim.

Three-Degree-of-Freedom Results

Motion Below Resonance

The total angle-of-attack history derived from the gyros is compared with the dynamic balance measurements for motion well below resonance in Fig. 5. Planar-type motion about trim existed for this test at a roll rate of approximately 155 deg/s which produced a roll to aerodynamic frequency ratio of $\Delta\omega/\omega_o \cong 0.3$.

Agreement between the two sets of angle of attack is quite good, including the pronounced "beating" of the maximum and minimum values resulting from the effect of the nose asymmetry. Body-fixed angle-of-attack cross plots transformed from the wind-fixed results[11] indicate an amplified trim angle of approximately 1.6 deg, which is consistent with Nelson's (tricyclic) analysis.[12]

Gyro-derived total out-of-plane moment coefficients (C_n) as a function of roll angle are compared with static values

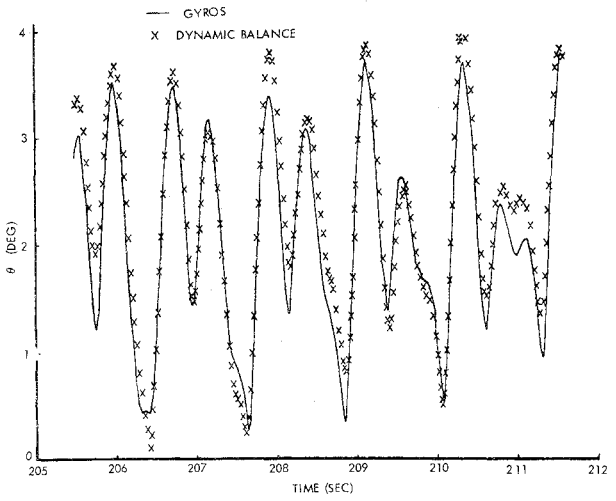

Fig. 5 Total angle-of-attack history, $\Delta\omega/\omega_o = 0.3$.

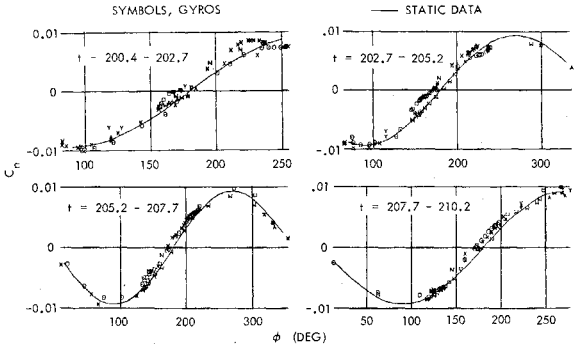

Fig. 6 Total out-of-plane moment coefficient, $\Delta\omega/\omega_o = 0.3$.

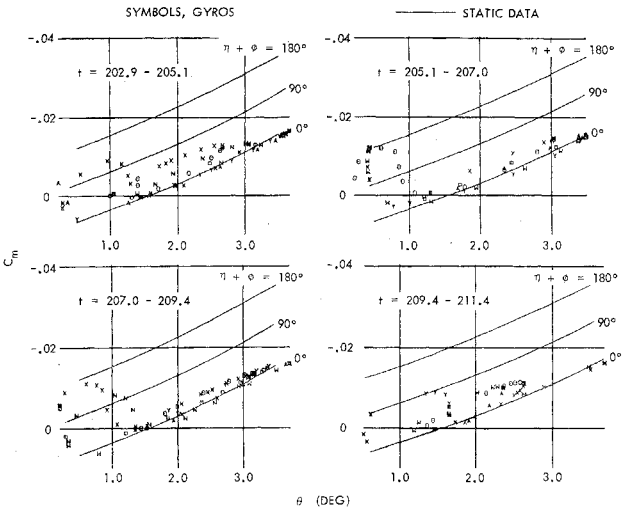

Fig. 7 Total in-plane moment coefficient, $\Delta\omega/\omega_o = 0.3$.

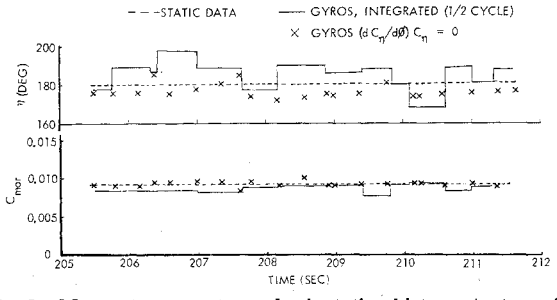

Fig. 8 Moment asymmetry and orientation history, $\Delta\omega/\omega_o = 0.3$.

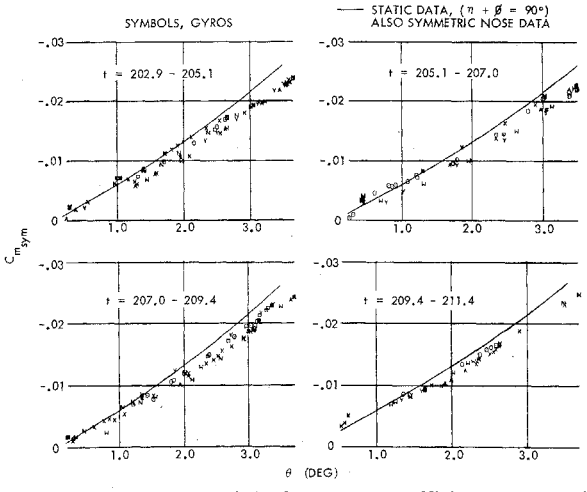

Fig. 9 Equivalent symmetric body moment coefficient, $\Delta\omega/\omega_o = 0.3$.

during the time interval of 200.4 to 210.2 s in Fig. 6. Although some scatter is indicated, generally good agreement exists between sets of data magnitudes and trends. Total in-plane moment coefficient (C_m) results as a function of total angle of attack are correlated with static moment results in Fig. 7. The three branches of the static moment curve correspond to the angle of attack 1) in the trim plane ($\eta + \phi = 0$), 2) 90 deg to the trim plane ($\eta + \phi = 90$), and 3) 180 deg to the trim plane ($\eta + \phi = 180$). In general, the results appear to follow the $\eta + \phi = 0$ branch, particularly for $\theta > \theta_{\text{trim}}$. However, significant ϕ variations for this nonlunar motion test cause difficulty in assessment of the gyro derived in-plane moment accuracy. An alternate approach for validating the accuracy would consist of extracting the moment asymmetry contribution from the total in-plane moment, thereby providing an equivalent symmetric body moment that will be independent of ϕ. A discussion of results obtained with this procedure follow the discussion of the moment asymmetry derivation.

The moment asymmetry C_{mor} and orientation angle η are compared with the static data in Fig. 8. Included are the gyro-derived results obtained by integrating Eq. (5) over one-half cycle and also the "instantaneous" values using the derivative form, Eq. (8); good agreement between the data is indicated.

An equivalent symmetric body moment curve as a function of angle of attack is compared with static results for the symmetric nose configuration (symmetric body) and the asymmetric nose configuration oriented 90 deg to the trim plane ($\eta + \phi = 90$ deg) in Fig. 9. Equation (4) was used together with gyro-derived C_m, ϕ; a faired curve of the integrated C_{mor}, η results. Note that the static moment results for the symmetric body are identical to the asymmetric body static moments obtained for $\eta + \phi = 90$ deg, consistent with the assumptions imposed on Eq. (4). Although the $C_{m_{\text{sym}}}$ values derived from the gyro analysis are somewhat low, a reasonable approximation to the symmetric body moments is indicated, thus aiding considerably in interpretation of these results compared with the total in-plane moment coefficients (Fig. 7). The consistent results obtained using this approach serve to verify the gyro analysis technique.

Motion Approaching Resonance

Comparison of the gyro-derived and dynamic balance total angle-of-attack history for motion approaching resonance is shown in Fig. 10. Elliptic-type motion about trim is prevalent for this run at an approximate roll rate of 300 deg/s, producing a resonance frequency ratio of $\Delta\omega/\omega_o \cong 0.6$. Excellent agreement between the integrated and measured results is demonstrated, including the secondary oscillations about

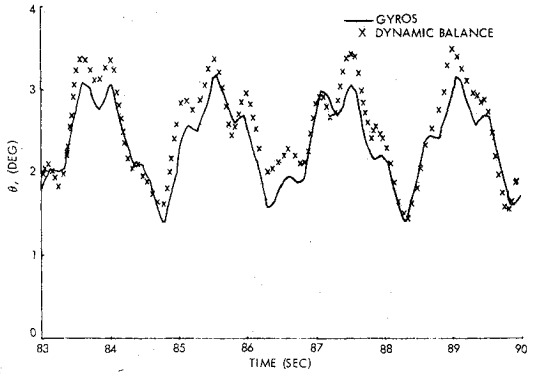

Fig. 10 Total angle-of-attack history, $\Delta\omega/\omega_\theta = 0.6$.

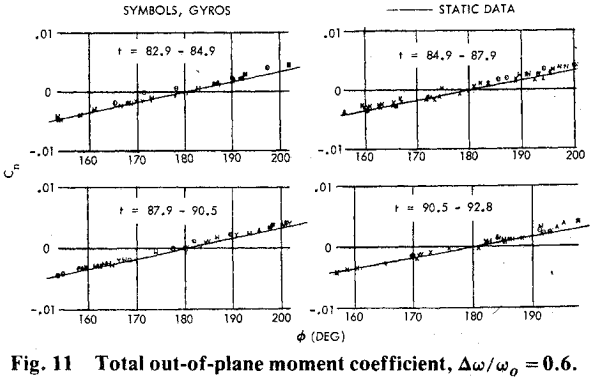

Fig. 11 Total out-of-plane moment coefficient, $\Delta\omega/\omega_o = 0.6$.

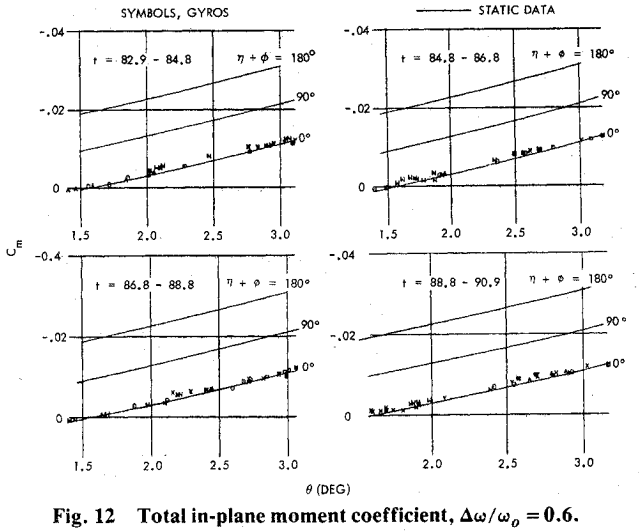

Fig. 12 Total in-plane moment coefficient, $\Delta\omega/\omega_o = 0.6$.

the primary waveform. An amplified trim angle of approximately 2.3 deg was obtained from the transformed body-fixed angle-of-attack cross plots,[11] reasonably correlating with results from Nelson's analysis of 2.1 deg.[12]

The out-of-plane moment coefficient (C_n) as a function of roll angle (shown in Fig. 11) depicts only a small portion of the sine wave exhibited in Fig. 6 as a consequence of the lunar motion pattern with small roll angle excursions from the trim plane. Excellent correlation with the static data is indicated. Gyro-derived in-plane moment (C_m) coefficient variation with angle of attack (Fig. 12) clearly illustrates essentially trim plane behavior. Close agreement with the static moment for the $\eta + \phi = 0$ (trim plane) branch is demonstrated.

C_{mor} and η histories derived from the gyro analysis are compared with static results in Fig. 13. Excellent correlation with the derivative expression, Eq. (8), is demonstrated, consistent with the out-of-plane moment results; however,

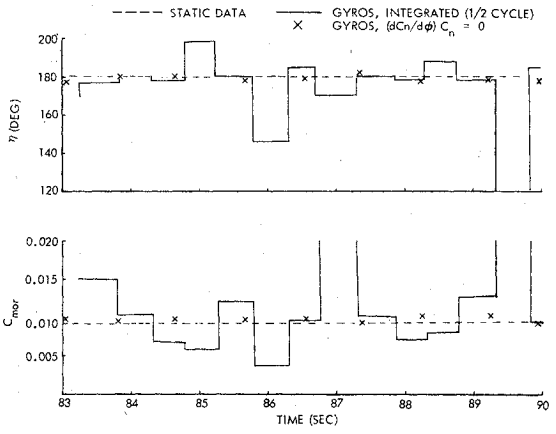

Fig. 13 Moment asymmetry and orientation history, $\Delta\omega/\omega_o = 0.6$.

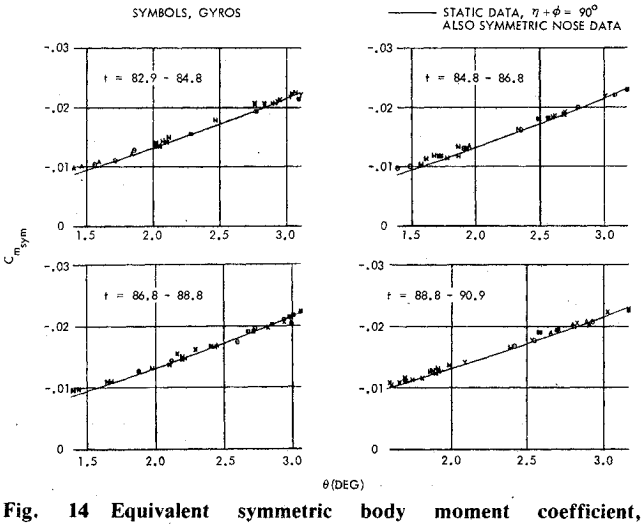

Fig. 14 Equivalent symmetric body moment coefficient, $\Delta\omega/\omega_o = 0.6$.

significant scatter in C_{mor} and η is obtained using the integral expression. These erratic results are attributed to the small change in ϕ over the time interval associated with this type of motion.

An equivalent symmetric body moment curve is presented in Fig. 14 as a function of total angle of attack. The input C_{mor}, η characteristics were faired results obtained using the derivative method. Excellent agreement with the static moment curve for a symmetric body is indicated.

Motion Above Resonance

Total angle-of-attack histories derived from the dynamic balance and gyro results are compared in Fig. 15 for motion well above resonance. Circular motion about trim is demonstrated at a roll rate of approximately 850 deg/s, providing a resonance ratio of $\Delta\omega/\omega_o \cong 1.8$. Generally good agreement between the two sets of data is indicated. Nelson's analysis[12] provided an amplified trim angle of 0.75 deg located 180 deg to the static orientation, which compares favorably with the effective trim of 0.65 deg with the same orientation, determined from transformed body fixed angle-of-attack crossplots.[11]

Out-of-plane moment gyro results (Fig. 16) demonstrate the sinuosidial variation with ϕ consistent with a rotary windward meridian. Good agreement with static test data is illustrated, with a slightly larger C_n derived from the gyro results. In-plane moment results (C_m) presented in Fig. 17 as a function of θ illustrate the effect of a rotary windward meridian. Moment coefficients show large "apparent" scatter between the extreme branches of the static moment results. Interpretation of the results in this form is difficult.

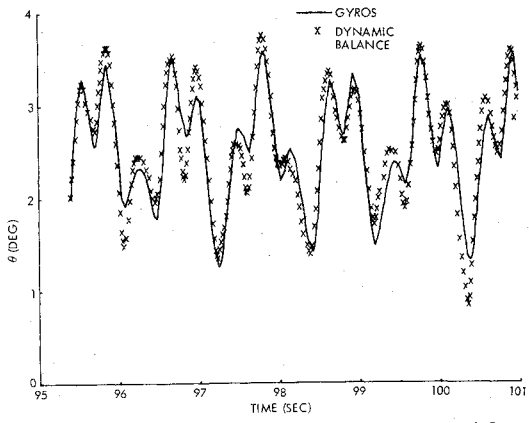

Fig. 15 Total angle-of-attack history, $\Delta\omega/\omega_o = 1.8$.

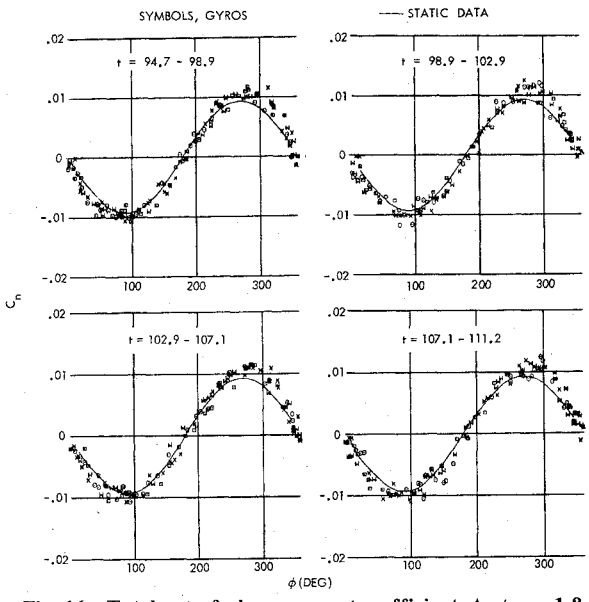

Fig. 16 Total out-of-plane moment coefficient, $\Delta\omega/\omega_o = 1.8$.

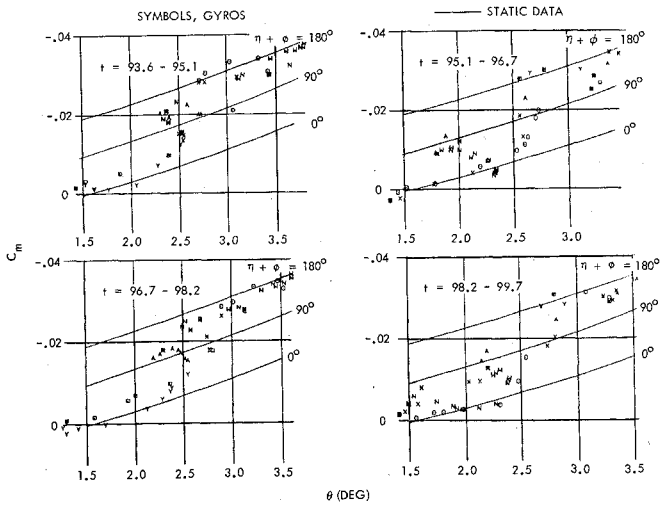

Fig. 17 Total in-plane moment coefficient, $\Delta\omega/\omega_o = 1.8$.

Gyro-derived C_{mor}, η histories using both the derivative and integrated methods, (Fig. 18) agree reasonably well with the static data. A somewhat larger asymmetry magnitude is indicated, consistent with the higher C_n values obtained from the gyro results.

Equivalent symmetric body moment results (Fig. 19) were obtained using averages of the C_{mor}, η results derived from

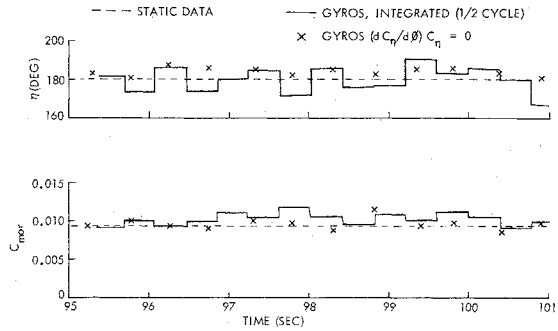

Fig. 18 Moment asymmetry and orientation history, $\Delta\omega/\omega_o = 1.8$.

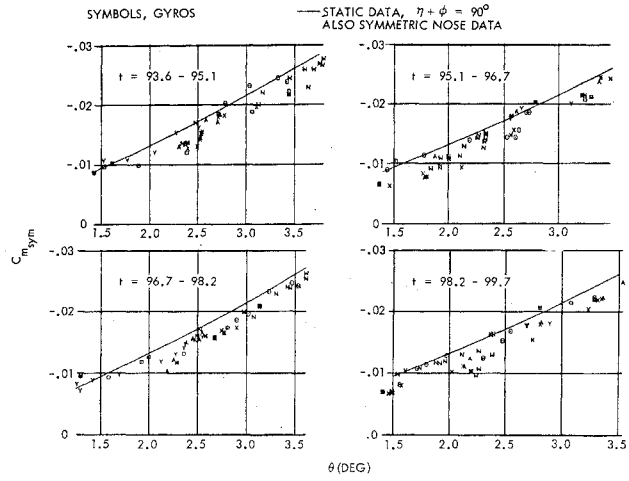

Fig. 19 Equivalent symmetric body moment coefficient, $\Delta\omega/\omega_o = 1.8$.

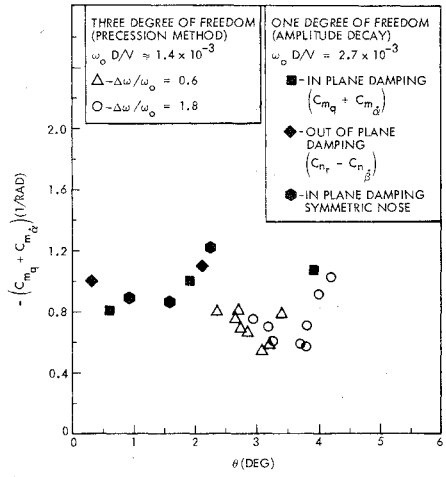

Fig. 20 Damping coefficient comparisons.

the integral method. Reasonable correlation with the static symmetric body results is demonstrated using this approach, which serves to identify the strong influence of the moment asymmetry term $[C_{mor}\cos(\eta+\phi)]$ on the in-plane moment data.

Damping Coefficient

Damping coefficients were obtained for the test runs approaching and above resonance using an integrated form of Eq. (5) applied over 10-s data intervals.[13] A mean of the maximum and minimum envelopes was used for the integrated average precession term in conjunction with the slope of the maximum precession term envelope in the evaluation. The contribution of a (constant) moment asymmetry term was

neglected in affecting the long-period precession term behavior. Results from this analysis as a function of the mean angle of attack are presented in Fig. 20. Experimental results obtained from a one-degree-of-freedom dynamic test at approximately twice the reduced frequency for both in-and out-of-plane damping are compared with the gyro-reduced damping coefficients. In general, the agreement is good; however, the effect of reduced frequency cannot be isolated for a direct comparison. Included for reference in Fig. 20 are one-degree-of-freedom dynamic test results for the symmetric nose configurations which agree well with the asymmetric nose data.

Significant effects of the moment asymmetry term on the precession term behavior for the test run ($\Delta\omega/\omega_o \cong 0.3$) provided no "apparent" damping for 50 s.

Concluding Remarks

Flight gyro hardware provides sufficient accuracy for angle-of-attack and detailed aerodynamic moment analysis. Angle-of-attack histories derived from the onboard rate gyro data agree well with the measured angular data from the dynamic balance, confirming the technique of correcting the gyro data for drifts. In- and out-of-plane moments directly obtained from gyro data compare well with results of a static test. Damping coefficients derived from the precession term behavior for two runs of the three-degree-of-freedom tests show reasonable agreement with one-degree-of-freedom dynamic results. For one test run, described as planar type motion about trim, the asymmetric nose produced an oscillatory positive/negative precession behavior which resulted in an "apparent" lack of damping.

An analysis method is presented for configurations described as basic symmetric bodies with small aerodynamic asymmetries. The *static* moment asymmetry and its *static* orientation derived from out-of-plane results for the asymmetric nose configuration agree well with measured static data. This agreement exists for cases above and below resonance roll rates. An equivalent symmetric body moment curve can be obtained from the asymmetric body moment results by removing the in-plane moment component of the asymmetry based on the derived moment asymmetry and orientation. This technique can aid considerably in interpreting moment results.

Acknowledgments

This work was sponsored by the Strategic System Project Office of the U.S. Navy. The author gratefully acknowledges the contributions made by the following LMSC personnel to this program: S. De Lu, W. Stake, J. Mandeville, R. Gibson, V. Levy, J. Wagner, B. Stone, and R. Rowher. Also appreciated are the efforts of G. Burt and H. Trolley of ARO Inc., associated with the Von Kármán Gas Dynamics Facility.

References

[1] Murphy, C.H., "Free Flight Motion of Symmetrical Missiles," BRL Report 1216, July 1963.

[2] Nicolaides, J.D. and Eikenberry, R.S., "Dynamic Wind Tunnel Testing Techniques," AIAA Paper 66-752, AIAA Aerodynamic Testing Conference, Sept. 1966.

[3] Vaughn, H.R., "A Detailed Development of the Tricyclic Theory," Sandia Laboratories, Albuquerque, N.M., SC-M-67-2933, Feb. 1968.

[4] Chapman, G.T. and Kirk, D.B., "A New Method for Extracting Aerodynamic Coefficients From Free Flight Data," *AIAA Journal*, Vol. 8, April 1970, pp. 753–758.

[5] Prislin, R.H. and Jaffe, P., "Evaluation and Extension of the Tricyclic Equation of Motion," AIAA Paper 68-386, AIAA 3rd Aerodynamic Testing Conference, San Francisco, Calif., April 8–10, 1968.

[6] Clark, E.L. and Hodapp, A.E. Jr., "An Improved Technique for Determining Missile Roll Rate With the Epicyclic Theory," AIAA Paper 70-536, AIAA Atmospheric Flight Mechanics Conference, University of Tennessee Space Institute, Tenn. May 13–15, 1970.

[7] Lusardi, R.J., Nicolaides, J.D., and Ingram, C.W., "The Determinination of Non – Symmetric Aerodynamics of Re-Entry Missiles," *Journal of Spacecraft and Rockets*, Vol. 12, April 1975, pp. 193–198.

[8] Chrusciel, G.T., "Analysis of Re-Entry Vehicle Behavior During Boundary-Layer Transition," Lockheed Missiles & Space Co., Inc., LMSC TM 81-11/80, Dec. 1973.

[9] Ward, L.K. Jr. and Hodapp, A.E. Jr., "A Three-Degree-of-Freedom Dynamic Balance for Use in the VKF Continuous Flow Hypersonic Tunnels ($M_\infty - 6$ through 12)," AEDC-TR-68-62 (AD 832300), May 1968.

[10] Levy, V.H., "Deconvolution of Data Using the General-Purpose L-B Digital Filter With Phase Characteristics," Lockheed Missiles & Space Co., Inc., LMSC TM 48-80, July 1975.

[11] Chrusciel, G.T., "Analysis of Hypersonic 3DOF Test Results Employing Onboard Rate Gyros (R-185)," Lockheed Missiles & Space Co., Inc., LMSC-D477727, TM 81-11/128, Dec. 1976.

[12] Nelson, R.L., "The Motions of Rolling Symmetrical Missiles Referred to a Body-Axis System," NACA TN 3737, Nov. 1956.

[13] Chrusciel, G.T., "Application of Plane Fixed Equations of Motion to Re-Entry Vehicle Flight Analysis," Lockheed Missiles & Space Co., Inc., LMSC TM 81-11/69, Aug. 1972.